Sādhanā, Vol. 26, Parts 1 & 2, February–April 2001, pp. 25–34. © Printed in India

Solidification microstructure development

G PHANIKUMAR and K CHATTOPADHYAY

Department of Metallurgy, Indian Institute of Science, Bangalore 560012, India
e-mail: kamanio@metalrg.iisc.ernet.in

Abstract. In the present article, evolution of microstructure during solidification, as a function of various parameters, is discussed. Macrosegregation is described as being due to insufficient diffusivity of solute in the solid. Pattern formation is discussed in the light of instabilities at the solidification growth front. An overview of the scaling relations for various microstructures is given. Metastable extensions to equilibrium phase diagrams and corrections to equilibrium quantities are described.

Keywords. Solidification; microstructure; pattern formation; metastability.

1. Introduction

A majority of manufacturing processes involve melting and solidification of metals and alloys during fabrication of various components. Primary manufacturing processes such as ingot casting, continuous casting, squeeze casting, pressure casting and atomization, and secondary manufacturing processes such as welding, soldering, brazing, cladding and sintering, involve solidification as an important stage of the process. Thermal and solutal conditions that prevail during the process and thermodynamic and kinetic constraints of the material determine the final microstructure. The mechanical or functional properties and the microstructure of the various phases in turn dictate the performance of the final product.

Solidification involves the extraction of heat from the liquid and the motion of the solid–liquid interface. The rate of solidification is determined mainly by heat extraction through thermal diffusion and convection. However, solidification microstructure is a complex function of the rate of solidification (v), temperature gradients (G), composition (C) and several material characteristics such as phase equilibrium reactions, nucleation and growth kinetics of the phases and crystallographic constraints. A perspective of evolution of microstructure during solidification is presented in the light of our current understanding of solidification processing. Particular attention is paid to the effect of system size and resultant scale dependence of the microstructure and segregation profile. We emphasize the fact that our current knowledge allows us to have quantitative understanding.

2. System scale

Consider a directional solidification setup as shown in figure 1. Thermal flux balance at the solidification interface leads to the relation:

$$K_S G_S - K_L G_L = rLv\,. \tag{1}$$

Here, K_S and K_L are thermal conductivities and G_S and G_L, thermal gradients in solid and liquid, and r, L and v are density, latent heat and solidification rate respectively. Neglecting the situation of a highly undercooled melt, when the temperature gradient in the liquid is negative, the highest directional solidification rate achievable for a given system size is limited by the conduction mode heat removal by the solidified metal alone and is given by,

$$n_{\mathrm{MAX}} = K_S G_S / rL. \tag{2}$$

Equation (2) assumes no resistance to heat transfer. For a casting process, heat transfer through the surrounding mould is a limiting factor. In this case, (2) needs to be modified by incorporating resistance to heat transfer by the mould. In this case, solidified thickness or the modulus of solidification (V/A) is related to the solidification time by,

$$\frac{V}{A} = \frac{T_M - T_0}{r_S L}\left(\frac{2}{p^{1/2}}(K_M r_M C_M)^{1/2}(t_f)^{1/2} + n\frac{K_M t_f}{2r}\right). \tag{3}$$

Here the subscript M represents mould, V and A represent volume and area of the mould, r the radius of curvature of the mould, and n is a geometric constant. The time for completion of solidification is t_f and T_0 is the initial liquid temperature. As one can see, the equation consists of terms outside the bracket that are controlled essentially by the material properties. The first term in the bracket reflects the properties of the mould while the second term reflects the geometry. The term n takes different values depending on the geometry of the casting, and thus influences the solidification process. For example, a spherical mould ($n = 2$) solidifies faster than a cylindrical mould ($n = 1$).

For a conducting mould, the main resistance to heat transfer occurs at the mould–metal interface. In such a case (for example, chill casting), the solidification thickness (S) is

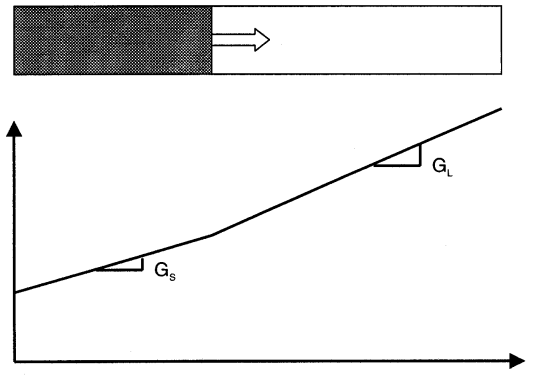

Figure 1. Schematic of directional solidification.

limited by the heat transfer coefficient h across the metal–mould interface. A simple heat transfer analysis allows us to obtain the following governing equation for this case,

$$S = t_f h(T_M - T_0)/r_S L. \tag{4}$$

Thus the rate of solidification becomes a function of the thermal parameters of the process and the materials properties. However, it should be noted that in processes such as the Bridgeman technique, growth rate and temperature gradient can be controlled independently. This enables study of these two important parameters on solidification microstructure and properties (Flemings 1974).

3. Segregation

Equilibrium solidification assumes that the solid-liquid interface moves at an infinitesimally slow pace such that the thermal and the solutal fields redistribute to adjust to the temperature and the composition values given by the equilibrium phase diagram. However, as can be gathered from the previous section, the solidification speed (v) is finite. The scale of the system for this to happen is given by,

$$D_s \gg L_X n. \tag{5}$$

Here, L_X is the system length scale in one dimension and D_S is the solute diffusivity in solid. Thermal and solutal diffusivities are finite and usually very small. This imposes a limit on the system scale to qualify for equilibrium solidification. Substituting typical diffusivities (thermal: 10^{-4} cm^2/s, solutal: 10^{-6}cm^2/s), for a system size of 1 cm, the solidification rate should be below 10^{-6}cm/s, a very small value. Most of the solidification processes in reality are at rates of about three orders of magnitude larger. As a result, the solutal field equilibration is not achieved and microsegregation patterns will result.

The composition of the liquid C_L left over after a fraction f_L has solidified from a liquid of initial composition C_0 is now no longer be given by the equilibrium lever rule. This problem has been resolved by Scheil (1942). The formulation assumes no solid diffusivity and infinite liquid diffusivity. The concentration of the liquid in this case is given by,

$$C_L = C_0 f_L^{(k-1)} \tag{6}$$

Here, k is the solute partition coefficient (C_S/C_L) which depends on the nature of the phase diagram. This is popularly known as Scheil's equation or non-equilibrium lever rule. A modification of this equation to incorporate finite diffusivities of solid as well as liquid gives the following expression which is valid for large systems (Bower *et al* 1966),

$$C_S^* = kC_0\left[\frac{a}{k-1} + \left(1 - \frac{ak}{k-1}\right)(1 - f_S)^{k-1}\right], \tag{7}$$

where,

$a = -D_L G/(m_L n C_0)$ and m_L is the slope of the liquidus.

For large system scales, the solute field in the liquid itself might not be uniform due to convection and the solute content of the solid formed at various locations in the system might be non-uniform, resulting in macrosegregation (Flemings 1974).

4. Microstructure evolution

In the previous sections we have discussed about the rate of solidification and composition profiles that come about at the system scale. However, as the solidification proceeds, the solid–liquid interface could undergo perturbations and develop instabilities that lead to the final microstructure of the solid.

4.1 *Cellular pattern*

For a pure metal, a positive thermal gradient in the liquid leads to a stable plane front solidification and a negative thermal gradient in the liquid leads to instability of plane front giving rise to 'thermal dendrites' that are not distinguishable by microstructural analysis.

Consider a thermal gradient situation, as in figure 2, for an alloy. A small perturbation on the interface for the stable interface (figure 2c) will 'see' temperature higher than the liquidus temperature and hence will melt back. Thus the stability of the flat interface will be maintained. But for the unstable interface (figure 2d), interface across a small perturbation 'sees' more undercooling at its location and grows further, leading to a

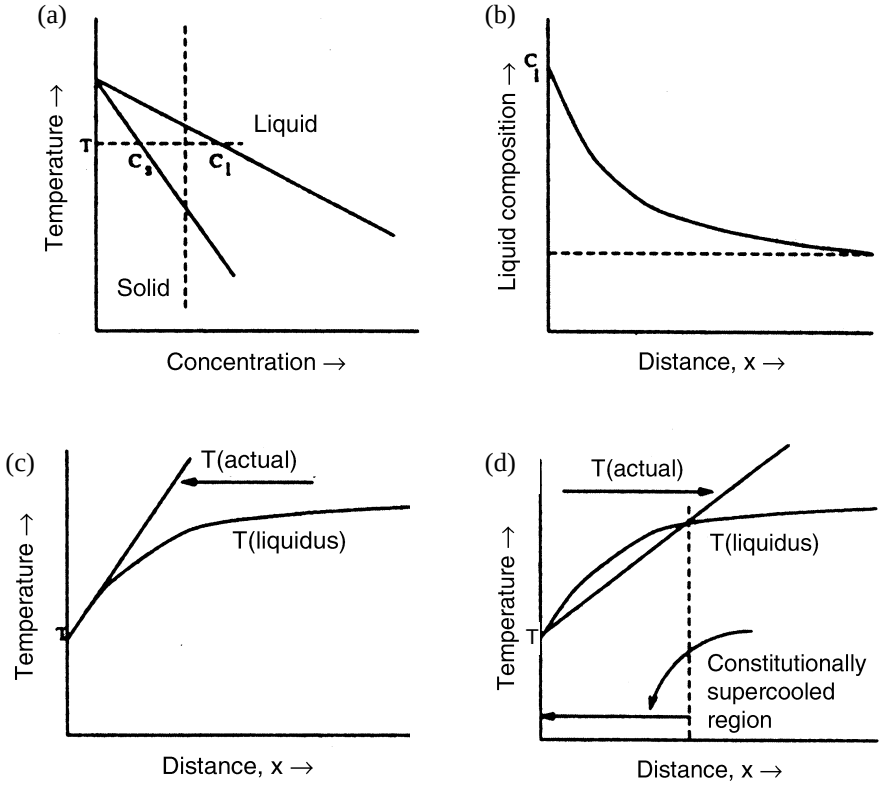

Figure 2. Schematic to indicate constitutional supercooling. (**a**) Phase diagram. (**b**) Solute-enriched layer in front of solid–liquid interface. (**c**) Stable interface. (**d**) Unstable interface.

breakdown of the planar front. The critical thermal gradient in the liquid at which such breakdown can take place is given by,

$$G_L/n \geq M_L C_0(1-k)/kD_L. \tag{8}$$

The microstructural patterns that form in this manner are termed 'cellular'. Hunt (1977) analysed the scale of these patterns (l) as a function of the thermal gradient G, and solidification speed v. This is given by,

$$nG^2 l^4 = 64qD[m(1-k)C_\infty + KGDn^{-1}]. \tag{9}$$

Here q is the curvature undercooling constant. At the critical condition for constitutional undercooling, the RHS of (9) tends to zero. Cellular pattern results if the system is away from the critical condition by an increase in v or C or by a decrease in G. The scaling relation given by (Hunt 1977).

$$nG^2 l^4 = -64qDm(1-k), \tag{10}$$

or in other words, $l \propto G^{-1/2}$ or $l \propto n^{-1/4}$.

In the foregoing discussion, we have assumed isotropy, i.e. that there is no preferred crystallographic orientation of easy growth and that shape of the interface is determined by the growth parameters. However, in several systems such as silicon, attachment kinetics are different along different planes leading to faceting of the growing front. Faceting behaviour is observed when the parameter a, popularly known as Jackson roughness parameter, given in the equation below, is above 2 (Jackson & Hunt 1965),

$$a = L_0 n^*/(k_B T_M N). \tag{11}$$

Here, L_0 is the latent heat per atom, n^* is the number of neighbors in the plane growing, k_B is the Boltzmann constant and N is the co-ordination number. Thus the faceting tendency depends upon both material parameters like latent heat and geometrical parameter of the growing plane and the crystal.

4.2 *Effect of surface tension on plane front solidification*

Although (8) is highly successful in predicting the onset of the interface breakdown during growth, this is not valid at high growth. At high growth velocity, the perturbation wavelengths become smaller. When the perturbations are small, surface tension plays an important role, comparable in magnitude to that of the solute field and can stabilize the plane front. Mullins & Sekerka (1963) assumed interface equilibrium, isotropic surface energy and no convection to obtain a thermal condition at which the plane front is stabilized by the surface tension. A simple form of the conditions for the interface stability can be written as,

$$\frac{G_L}{v} + \frac{r_L L}{2k_L} \geq -\frac{m_L C_0(1-k)}{kD_L}\frac{K_S + K_L}{2K_L} y \ , \tag{12}$$

where y is a dimensionless stability function = f(A),

$$A = -k^2 gnT_M/[(1-k)r_L D_L m_L C_0].$$

The value of y can be obtained from the table given by the authors and provides a simple way to test the stability of the interface at high solidification rates. There now exists a rich collection of experimental findings which points to the correctness of this approach.

4.3 *Dendritic pattern*

Anisotropy of surface tension and instabilities at the growing tip of the cell can lead to side branching. A cell with side branches resembles a tree and so is termed 'dendrite'. While the growth direction of cells is determined by the maximum thermal gradient, the growth direction of dendrites deviates from it. It is a compromise between the direction of maximum thermal gradient and of the crystallographic easy growth, which is $\langle 100\rangle$ for FCC and BCC and $\langle 10\bar{1}0\rangle$ for HCP (Billia & Trivedi 1993).

Dendrite tip temperature (T_D), modified by the presence of nonequilibrium compositions at the interface and the curvature, is given as

$$T_D = T_M + m_V C_L - \Delta T_C. \tag{13}$$

Here, m_V is the liquidus slope modified for the solidification velocity v, C_L is the liquid composition and DT_C is the curvature undercooling.

The curvature at the tip of a dendrite can be seen as due to a pressure field and the resultant decrease in the freezing temperature is given by the Gibbs–Thomson relation.

$$\Delta T_C = gk/\Delta S. \tag{14}$$

Here, g is surface tension, k is curvature of interface and ΔS is entropy of fusion per unit volume.

Kurz & Fisher (1981) have modelled the dendritic growth assuming that the dendrite tip is a hemisphere with radius equal to the wavelength of the critical instability of the solid–liquid interface. By minimizing the undercooling with respect to the radius of curvature of the tip, they have obtained steady-state growth velocity as given by,

$$v = \frac{2D(GR^2 + 4p^2\Gamma)}{R^3 rG - 2(1-k)C_0 m + 4p^2 R(1-k)}. \tag{15}$$

Here, R is the radius of the dendrite tip, and Γ is the surface tension. In the limiting cases, we observe the following behaviour.

At small v:

$$v = \frac{2DG}{R(1-k)G - 2(1-k)C_0 m}, \tag{15a}$$

$$R = \frac{2D}{v(1-k)} + \frac{2mC_0}{G}. \tag{15b}$$

At large v:

$$v = \frac{4p^2 D\Gamma}{R^2(1-k)C_0 m}, \tag{15c}$$

$$R = 2p[(D\Gamma/nk\Delta T_0)]^{1/2} \tag{15d}$$

$$\Delta T_0 = -mC_0(1-k)/k, \tag{15e}$$

i.e., at small growth rates, the radius declines rapidly with increasing growth rate and at large growth rates, the radius falls parabolically with increasing growth rates.

Assuming the overall morphology of the dendrite to be ellipsoidal, the primary dendrite spacing d is obtained as,

For small v:

$$d = \left[\frac{6\Delta T'}{G(1-k)}\left(\frac{D}{v}\right) - \frac{\Delta T_0 k}{G}\right]^{1/2}. \tag{16a}$$

For large v:

$$d = 4{\cdot}3\Delta T' 1/4(D\Gamma/\Delta T_0 k)^{1/4} n^{-1/4} G^{-1/2}, \tag{16b}$$

where,

$$\Delta T' = \frac{\Delta T}{(1-k)}\left(1 - \frac{GD}{v\Delta T_0}\right)$$ and DT is the undercooling.

The secondary arm spacing l_2 is one of the most important length scales of dendritic microstructure since it determines the periodicity of solute segregation profile in the solidified material and thus influences its properties. The side branches become stable when the solute diffusional effects for instability are balanced by the stabilizing effect of the surface tension. It turns out that the secondary arm spacing is a geometric mean of the length scales of the thermal, solutal and capillarity fields (Trivedi & Kurz 1994).

$$l_2 = (l_D l_C d_0)^{1/3}. \tag{17}$$

Here, l_D is the thermal diffusion length, l_C is the solute diffusion length and d_0 is the capillarity length.

4.4 *Eutectic growth*

In the discussion above, we have considered one solid phase growing in to liquid under various thermal conditions. However, in eutectic alloy systems two solid phases grow in to a liquid simultaneously. The microstructure exhibited by the eutectic solids is also varied. They can be classified as regular eutectic with lamellar or rod morphology and irregular eutectic showing no regularity of distribution of the two phases. Regular eutectic growth is modelled by Jackson & Hunt (1966) who solved the solute diffusion equation for a steady state growth at minimum undercooling. The resultant equation gives a relation between the undercooling, growth rate and eutectic spacing (Jackson & Hunt 1966),

$$\Delta T/m = n\,l\,Q + (A/\,l), \tag{18a}$$

$$Q = P(1+V)^2 \mathrm{C}_0/VD, \tag{18b}$$

$$A = 2(1+V)(a_a^L / m_a)/(a_b^L / m_b), \tag{18c}$$

$$V = S_a/S_b \tag{18d}$$

where, m is the harmonic mean of the liquidus slopes for a and b phases, P is a function of the volume fraction, S_a and S_b are the half-spacings of the lamellae/rods and a_a^L and a_b^L, the Gibbs–Thompson coefficients of a and b phases respectively.

Assuming that the solid grows at the maximum growth rate for a given undercooling, the eutectic spacing, velocity and undercooling are related as:

$$l^2 n = A/Q, \tag{19a}$$

$$\Delta T^2/n = 4m^2 AQ, \tag{19b}$$

$$\Delta T l = 2mA. \tag{19c}$$

The above analysis is successful in predicting the lamellar or rod spacings under different growth conditions as well as the shape of the solid–liquid interface. This also explains the transformation of the lamellar eutectic to rod eutectic at low volume fraction. The analysis of the other eutectic morphologies is more complex. Although progress has been made in these directions, we shall not discuss them in the present article.

5. Non-equilibrium effects

5.1 *Effect of convection*

Although most of the models in the solidification literature have been developed under the assumption that the liquid is static, in real systems convection cannot be ignored. Convection enhances transport of heat and species, thereby introducing a correction to thermal and solutal diffusivity. Enhanced diffusion helps in the coarsening of microstructures and the final pattern spacing falls into a band of values rather than a single selected value. Convection also influences morphological instability and interface structure. There have been observations on massive transparent specimens revealing that convection results in a gradient of microstructure along the interface from smooth interface to dendrites (Boettinger *et al.* 2000).

5.2 *Correction to partition coefficient*

Finite diffusivity of species does not ensure partitioning of species across the solid–liquid interface at high growth rates. The effective partition coefficient has to be corrected by the velocity of the interface. Aziz (1982) derived an expression for this corrected partition coefficient as in (18). This expression has important consequences such as extended solid solution formation at high growth rates. In the limit of velocity taking a high value in comparison with the diffusion limited velocity, the partition coefficient tends to unity, resulting in complete solute trapping,

$$k^* = (k + n_i/v_D)/(1 + n_i/n_D), \tag{20}$$

where v_i is the interface velocity, v_D is the interface characteristic diffusion velocity, k^* is the corrected partition coefficient.

5.3 *Metastable phase diagram*

At high growth rates, if nucleation of equilibrium phases gets suppressed due to insufficient time, metastable phase formation is possible. Modifications to the phase fields in the equilibrium phase diagram are required. As an illustration, we can consider the case of TiNi alloy with about 0.3 wt% silicon. Silicon is known to promote icosahedral co-ordination in undercooled Ti–Ni melts and thus increases the nucleation of the Ti_2Ni phase. Ti_2Ni has a crystal structure that can be described as a packing of eight distorted icosahedra. A rapid solidification route such as melt spinning leads to large undercooling ($\Delta T/T_M \sim 0{\cdot}4$) that suppresses nucleation of equilibrium phases. Thus, nano dispersions of Ti_2Ni phase are observed to form during melt spinning of Ti–Ni alloy though the equilibrium phase diagram shows no formation of this phase from equiatomic melts. A calculated phase diagram of TiNi to incorporate metastable extension to the Ti_2Ni phase field is shown in figure 3 (dashed line) (Nagarajan & Chattopadhyay 1994).

In the limit of rapid solidification, nucleation of a crystalline phase formation itself could be suppressed and the liquid could freeze as a glass. These amorphous alloys exhibit fascinating properties such as high elastic modulus, high corrosion resistance and high strength and toughness. Production of such metallic glasses in a bulk form is presently one of the active areas of research in materials science.

As we can gather from our discussion, the kind of phases that grow into the liquid, and their morphology, is a strong function of processing parameters such as growth rate, thermal gradient and composition. It is possible that one could develop a solidification map with processing parameters along the axes and phases and their morphologies marked in various domains. Gill & Kurz (1995) have demonstrated this by developing an Al–Cu solidification microstructure map (Gill & Kurz 1995).

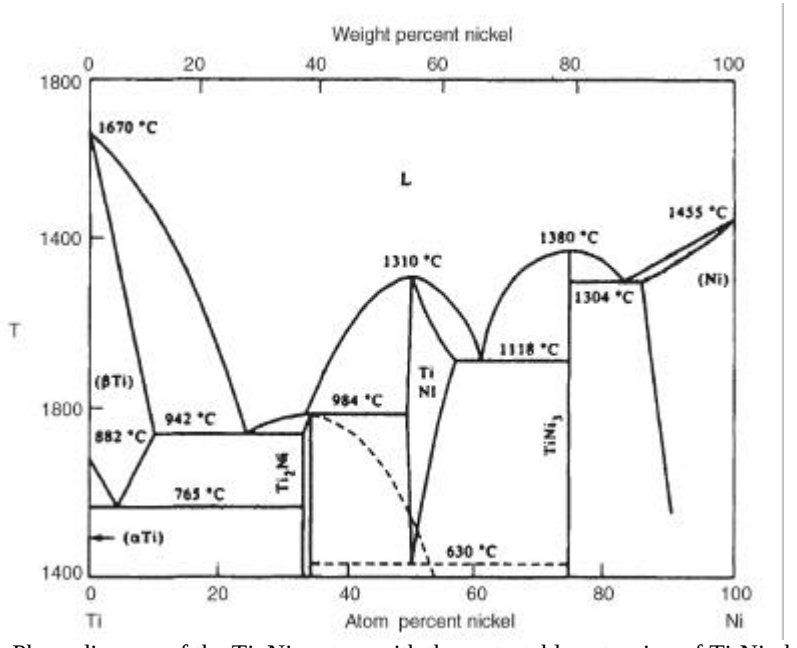

Figure 3. Phase diagram of the Ti–Ni system with the metastable extension of Ti_2Ni phase field.

6. Conclusions

From the above discussions, it is clear that most of the solidification processes can now be understood at basic level. Quantitative relations are now available which can predict the development of the microstructure under different solidification conditions. In fact, several commercial softwares are now available that predict the microstructure of the processed samples and are extensively used in the design of castings. In recent times, emergence of the phase field technique and fast computers raises the hope of computationally studying the evolution of microstructure during solidification with very few assumptions. Thus, it appears that the field of solidification processing has reached maturity and is now only a matter of incorporating the available knowledge in process control. This line of argument, widely circulated in the international research arena by some leading experts in the field, is however fraught with great danger. Although the progress is impressive, it is prudent to remember that our ability to model nucleation is still not satisfactory. Almost all the growth models also ignore the issues of convection and complex fluid flow that affect the evolution of the microstructure. Admittedly, a great deal of understanding has been achieved for pattern formation and microstructure development. However, beautiful patterns in complex alloys which surprise a solidification researcher and raise hope of new properties still emerge unexpectedly. Thus, the field is expected to remain vibrant for researchers and engineers in the near future.

References

Aziz M J 1982 Model for solute redistribution during rapid solidification. *J. Appl. Phys.* 53: 1158–1168

Billia B, Trivedi R 1993 Pattern formation in crystal growth. *Handbook of crystal growth* (ed.) D T J Hurle (Amsterdam: Elsevier) 1: 899–1073

Boettinger W J, Coriell S R, Greer A L, Karma A, Kurz W, Rappaz M, Trivedi R 2000 Solidification microstructures: Recent developments, future directions. *Acta Mater.* 48: 43–70

Bower T F, Brody H D, Flemings M C 1966 Measurements of solute redistribution in dendritic solidification. *Trans. Metall. Soc. AIME* 236: 624–634

Flemings M C 1974 *Solidification processing* (New York: McGraw-Hill)

Gill S C, Kurz W 1995 Rapidly solidified Al–Cu alloys – II. Calculation of the microstructure selection map. *Acta Metall. Mater.* 43: 139–151

Hunt J D 1977 Cellular and primary dendrite spacings. *Sheffield International Conference on Solidification and Casting,* Ranmoor House, Sheffield University 1: 1–26

Jackson K A, Hunt J D 1965 Transparent compounds that freeze like metals. *Acta Metall.* 13: 1212–1215

Jackson K A, Hunt J D 1966 Lamellar and rod eutectic growth. *Trans. Metall. Soc. AIME* 236: 1129–1142

Kurz W, Fisher D J 1981 Dendrite growth at the limit of stability: Tip radius and spacing. *Acta Metall.* 29: 11–20

Mullins W W, Sekerka R F 1963 Morphological stability of a particle growing by diffusion or heat flow. *J. Appl. Phys.* 34: 323–329

Nagarajan R, Chattopadhyay K 1994 Intermetallic Ti_2Ni/TiNi nanocomposite by rapid solidification. *Acta Metall. Mater.* 42: 947–958

Scheil E 1942 *Z. Metallkunde* 34: 70

Trivedi R, Kurz W 1994 Solidification microstructures: A conceptual approach. *Acta Metall. Mater.* 42: 15–23